Tumor Detection Based on Spatial and Inter-Slice Analyses for MRI Breast Imaging

Guo-Shiang Lin[1], S. K. Chai[2], Wei-Cheng Yeh[3], Lin-Jie Cheng[1]

[1]Dept. of Computer Science and Information Engineering, Da-Yeh University, Chang-Hua, Taiwan, R.O.C.
khlin@mail.dyu.edu.tw
[2]Dept. of Health Services Administration, China Medical University, Taiwan, R.O.C.
skchai@mail.cmu.edu.tw
[3]Radiology dept., Chia-Yi hospital, dept. of Health, Executive Yuan, Taiwan, R.O.C.
h0515@hotmail.com

ABSTRACT

In this paper, we propose a scheme composed of the spatial and inter-slice analyses to achieve tumor region identification in MRI breast images. Our spatial analysis evaluates the intensity and size information of candidate regions, while the inter-slice analysis is based on the continuity characteristic to verify the static behavior of tumor regions. To find a precise region, a region growing algorithm is proposed based on ellipse fitness. The experimental results show that our proposed scheme can correctly identify tumor regions.

1. INTRODUCTION

The mortality from breast cancer has been greatly increasing in Taiwan over the past two decades, and it has become the fourth leading cause of cancer death. According to a statistics investigated by The Department of Health, Taiwan [2], the death rate of female breast cancer rose from 3.9% in 1985 to 12.9% in 2005. It is critical, therefore, to detect breast cancer at an early stage since it will greatly improve the therapy and decline mortality [3]. Detection of breast cancer is often carried out by inspecting ultrasonography, mammography, or MRI images [4]-[7]. Ultrasonography is a popular method for breast cancer diagnosis, but its performance is limited to detect cystic lesions or advanced breast cancer [4]. Mammography is another widely used tool for breast cancer detection, and various computer-aided methods for this have been developed [4]-[6]. However, it is still a great challenge for mammography to detect lesions at an early stage. At this stage, the lesion size is quite small, and its brightness in the image is similar to that of tissues such as fat or gland, especially for eastern young people. In order to improve the early detection rate of breast cancer, healthcare organizations have been working on promotion of self breast examination, and the government has provided financial for ultrasound and mammography screening over

the past years. The progress, however, is unsatisfactory. A statistics shows that near about forty-five percent of breast cancer cases were found in stage 2 and one fourth of the breast malignancy cannot be removed surgically at the time when it is diagnosed.

While ultrasound and mammography have their weaknesses in screening ductal carcinoma in situ (DCIS), magnetic resonance imaging (MRI) has demonstrated its capability of early breast cancer detection. Studies have shown that MRI has higher sensitivity than mammography does [8]. This is especially true for young women and for those with dense breasts. In addition, MRI can also accurately determine tumor regions. These reasons motivate us to develop a tumor detection scheme for MRI.

Even with great advancement in image processing techniques, it is still a difficult problem to precisely detect a tumor boundary especially when the background is spoiled by soft tissues and noises. Traditional methods, such as Sobel and Laplacian operators, texture analysis, such as moments, and de-noising techniques can be used for achieving the tumor detection. However, considerations in complexity and robustness are challenging for this kind of techniques. Dissimilar to most of previous schemes, we adopt not only the spatial analysis in each MRI slice but also the inter-slice analysis to raise the detection performance, even there exists certain similarity in some tissue regions, e.g., vessels, in this paper. Experiments show that our scheme is capable of correctly detecting the tumor region.

2. THE PROPOSED SCHEME

Basically, to design a high efficient mechanism for tumor region detection in MRI breast images, we should first analyze characteristics of tumor regions. As we know, a MRI breast slice is basically composed of tumors and soft tissues. Though the composing components may be complicated, the tumor regions are characterized of high

intensity, size, and continuity between MRI slides. In this paper, based on these characteristics, we devise a tumor detection scheme composed of the spatial and inter-slice analyses. In the following, we will introduce the proposed algorithm in more details.

2.1 Spatial analysis

In the spatial analysis, the intensity and size information of tumor regions is utilized. Detailed steps are described below.

1. Morphological opening and automatic thresholding for tumor candidate selection

   Because the tumor regions have generally high intensity, morphological opening [1] is used here to split the background part and foreground part which contains the candidates of tumor regions. The foreground part can be obtained as

   $$f^R = f - (f \circ S), \qquad (1)$$

   where $\circ$ stands for the morphological opening operator, f denotes the original image, f^R represents the resulting version after morphological opening and subtraction, and S is the structure element in the morphological operator. After obtaining f^R, the automatic thresholding for selecting the candidates of tumor regions can be performed as follows:

   $$f^B(x,y) = \begin{cases} 1 & \text{if } f^R(x,y) > T^L, \\ 0 & \text{otherwise} \end{cases} \qquad (2)$$

   where f^B represents the output of automatic thresholding. T^L denotes the threshold to select 10% of pixels with high value after morphological opening.

2. Connected component labeling

   The chosen regions are labeled for the following processing. Actually, a labeled object may contain tumors and other tissues, e.g., vessels. Connected regions that have a size satisfying a given constraint (e.g., smaller that T^A) are identified for the following shape evaluation.

3. Shape refinement

   Although, the tumor candidate regions can be obtained after morphological opening, thresholding, and labeling, their regions may not be correctly detected. In addition, because the shape of tumor regions can be approximated by using an ellipse, survived connected regions should encounter an ellipse-shape test. Referring to [1], a method based on ellipse fitness was employed to find the correct tumor regions and measure their properties like center of mass, best-fit ellipse, etc. Figure 1 illustrates the measurement for ellipse fitness.

   To achieve shape refinement, a region growing algorithm is proposed and applied to each tumor candidate and described as follows.

(1) Compute the average intensity $\bar{I}_{B_i}$ and center of mass (x_c, y_c) of B_i as follows:

$$x_c = \frac{1}{|B_i^l|} \sum_{(x,y) \in B_i} x \quad, \quad y_c = \frac{1}{|B_i^l|} \sum_{(x,y) \in B_i} y \quad, \qquad (3)$$

where B_i^l denote the i-th candidate in the l-th iteration and $|B_i^l|$ represents the area of B_i^l.

(2) Measure $D(x,y)$ and $\beta(x,y)$ as follows:

$$\beta(x,y) = \frac{1}{2a_L} \sum_{i \in \{1,2\}} \sqrt{(x - x_f^i)^2 + (y - y_f^i)^2} \quad, \qquad (4)$$

$$D(x,y) = \beta(x,y) \sqrt{(I_{neighbor}(x,y) - \bar{I}_{B_i})^2} \quad, \qquad (5)$$

where $I_{neighbor}(x,y)$ is the neighboring pixel based on 8-connectivity, (x_f^i, y_f^i) denotes the coordinate of focus points of an ellipse. In Eq. (4), referring to [1], the major axe a_L is defined as

$$a_L = \left(\frac{4}{\pi}\right)^{\frac{1}{4}} \left[\frac{(I_{max})^3}{I_{min}}\right]^{\frac{1}{8}}, \qquad (6)$$

where

$$I_{min} = \sum_{(x,y) \in B_i} [(y - y_c)\cos\theta - (x - x_c)\sin\theta]^2 \quad,$$

$$I_{max} = \sum_{(x,y) \in B_i} [(y - y_c)\sin\theta + (x - x_c)\cos\theta]^2 \quad,$$

$\sin(\cdot)$ and $\cos(\cdot)$ represent sine and cosine functions, respectively, and θ denotes the orientation. According to Eqs. (4) and (5), as a pixel is near the focus points of an ellipse and its pixel value is closed to $\bar{I}_{B_i}$, $D(x,y)$ is small. This means the neighboring pixel with smaller $D(x,y)$ is similar to those pixels in this candidate.

(3) Include neighboring pixels as their $D(x,y)$ are less than T^D, where the threshold T^D is adjusted according to image content.

(4) Check whether the candidate overlaps the others. If this situation exists, then merge overlapped candidates, re-label all candidates, and jump to step (1).

(5) Check whether there are neighboring pixels to be processed by calculating $|B_i^D| = (|B_i^l| - |B_i^{l-1}|)$, where B_i^l and B_i^{l-1} represent the i-th candidate in the l-th and $(l-1)$-th slices, respectively. If $|B_i^D|$ is not zero, repeat step (1) to step (4); otherwise, stop.

2.2 Inter-slice analysis

In addition to the spatial analysis, inter-slice analysis is also performed to raise the accuracy of tumor region identification in this paper. Generally, the position of a tumor region may not change significantly during MRI slices. Based on this observation, we compare the center of mass between the recognized tumor regions of two test slices via checking

$$CT = \begin{cases} \text{true} & \text{if } \left(dist(p,q) < T^D\right) \wedge \left(B_i^l \cap B_i^{l-1}\right), \\ \text{false} & \text{otherwise} \end{cases} \quad (7)$$

where $\wedge$ is the logical AND operator, p and q denote the tumor regions from two test slices, $dist(p,q) = \sqrt{(x_c^p - x_c^q)^2 + (y_c^p - y_c^q)^2}$ is the Euclidean distance between their centers of mass, and T^D is a threshold. For each tumor region candidate B_i, the CT test is performed for all of MRI slices.

2.3 Tumor region identification

After spatial and inter-slice analyses, tumor regions can be all identified. For each MRI, if the number of CT of a recognized tumor candidate region is over a threshold T^t, this tumor region is thus identified. Otherwise, the candidate region is considered as noises.

3. EXPERIMENTAL RESULTS

To evaluate the performance of the proposed system, we use 2 MRIs captured in Taiwan. Each MRI has 128 slices and contains at least 1 tumor region. The slice size is 512×512 pixels. The first row of Figure 3, Fig.3 (a), Fig.3 (b), and Fig. 3(c), show the original MRI slices. After physician's suggestions, the size of structure element in the morphological opening is 25×25 pixels and T^A is set to be 625.

3.1 Spatial detection

The second row of Fig. 3, Fig.3 (d), Fig. 3(e), and Fig. 3(f), show the results of spatial analysis and the white window illustrates the true tumor region. As we can see in the second row of Fig. 3, there are some false alarm errors. The misclassification comes from several aspects. First, a false alarm often occurs as vessels exist. In addition, the shape of a vessel is ellipse-like. In addition, because the characteristics (e.g., size and intensity) of a vessel area satisfy these conditions of size and intensity, the vessel is considered as the tumor region.

3.2 Inter-slice analysis

The last row of Fig. 3, Fig.3 (g), Fig. 3(h), and Fig. 3(i), show the results of the spatial and inter-slice analyses. As

we can see in the last row, the true tumor can be correctly identified. Comparing to the second row of Fig.3, the false alarm errors are eliminated by using inter-slice analysis. That means that the continuity of the tumor region did exists and this property can be exploited to reduce interferences resulting from vessels or other tissues. The result shows that the performance of our proposed combing the spatial and inter-slice analyses can be raised.

4. CONCLUSION

In this article, we propose a scheme which contains the spatial and inter-slice analyses to achieve tumor region identification for MRI breast images. In the spatial analysis, the intensity and size information is utilized to find the candidates of tumor regions. To find a precise tumor region for further inspection, a region growing algorithm is proposed according to the intensity and distance information. In the inter-slice analysis, the characteristic of continuity of a tumor region among slices is exploited to remove noise resulting from other tissues and noises. The experimental results show that our proposed scheme can effectively identify the tumor region. The future work is to find more useful features (e.g., texture) to improve the proposed scheme. Besides, more MRI images are used to evaluate the performance of our proposed scheme.

REFERENCES

[1] A. K. Jain, *Fundamentals of Digital Image Processing*, Prentice Hall, 1989.

[2] Health and Vital Statistics, http://www.doh.gov.tw/statistic/, Department of Health, December 2006.

[3] R. M. Rangayyan, L. Shen, Y. Shen, J. E. Leo Desautels, H. Bryant, T. J. Terry, N. Horeczko, and M. S. Rose, "Improvement of sensitivity of breast cancer diagnosis with adaptive neighborhood contrast enhancement of mammograms," *IEEE Trans. on Information Technology in Biomedicine*, vol. 1, no. 3, pp. 161-170, Sep. 1997.

[4] T. Arodz, M. Kurdziel, T. J. Popiela, E. O.D. Sevre, and D. A. Yuen, "Detection of clustered microcalcifications in small field digital mammography," *Computer Methods and Programs in Biomedicine*, vol.81, pp.56-65, 2006

[5] S. Joo, Y. Seok, W. K. Moon, and H. C. Kim, "Computer-aided diagnosis of solid breast nodules: Use of an artificial neural network based on multiple sonographic features," *IEEE Trans. on Medical Imaging*, vol. 23, no. 10, pp.1292-1300, Oct. 2004.

[6] I. El-Naqa, Y. Yang, M. N. Wernick, N. P. Galatsanos, and R. M. Nishikawa, "A support vector machine approach for detection of microcalcifications," *IEEE Trans. on Medical Imaging*, vol. 21, no. 12, pp.1552-1563, Dec. 2002.

[7] M. L. Essink-Bot, A. J. Rijnsburger, S. van Dooren, H. J. De Koning, and C. Seynaeve, "Women's acceptance of MRI in breast cancer surveillance because of a familial or genetic predisposition," *The Breast*, vol. 15, pp. 673-676, 2006.

[8] E. A. Morris, "Screen for breast cancer with MRI," *Seminar in Ultrasound, CT, and MRI*, vol. 24, no. 1, pp.45-54, February 2003.
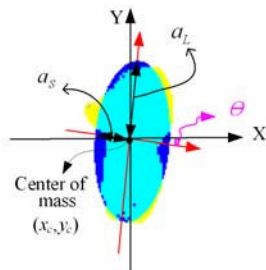
Fig. 1. An illustration for ellipse fitness
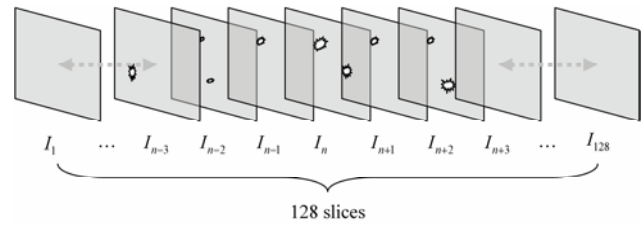
Fig. 2. An illustration of inter-slice analysis

(a)

(b)

(c)

(d)

(e)

(f)

(g)

(h)

(i)
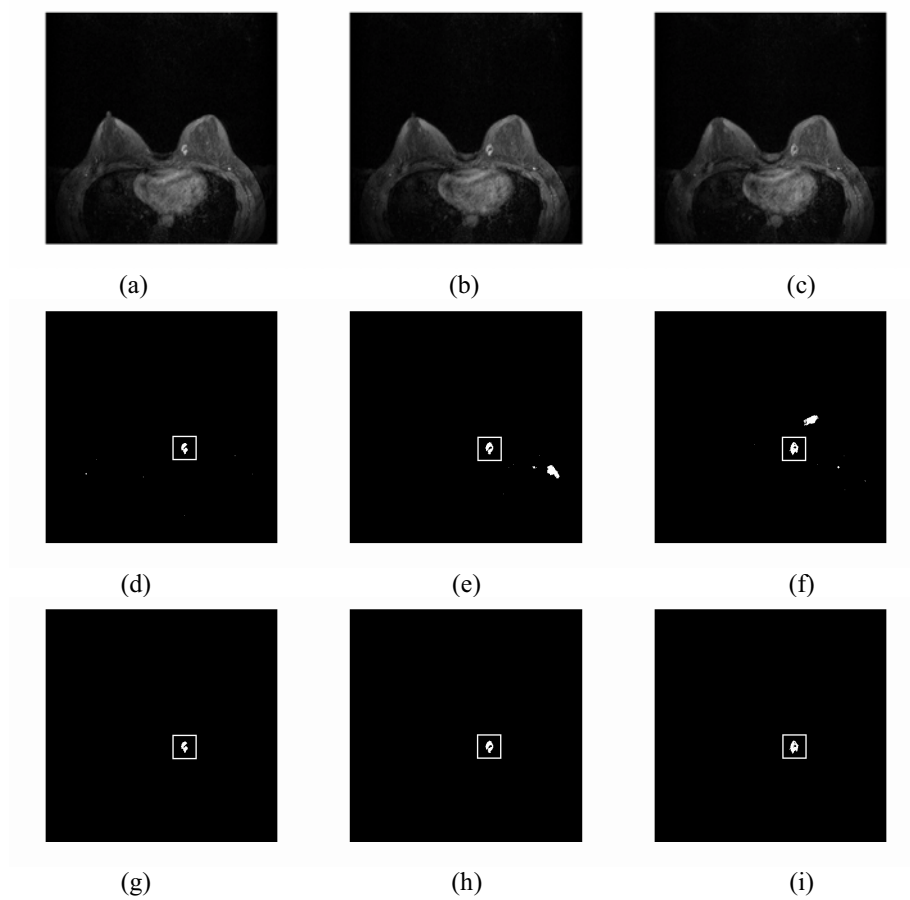
Fig. 3. Original MRI slices and detection results. (a), (b), and (c) are original MRI slices; (d), (e), and (f) are results of spatial analysis, (g), (h), (i) are the results after the spatial and inter-slice analyses.